Northern Hemisphere forcing of climatic cycles in Antarctica over the past 360,000 years

by K. Kawamura et al. (kawamura@nipr.ac.jp)

- **Supplementary Notes**

    Absence of climatic signal in O_2/N_2 records

    Error estimate for the DFO-2006 timescale

    Comparison with radiometric age markers

    Site temperature

- **Supplementary Tables S1-S3**

- **Supplementary Figures S1-S5**

- **References**

Absence of climatic signal in O_2/N_2 records

Using the DFO-2006 timescale, the correlation coefficient between Dome Fuji O_2/N_2 and local insolation is -0.89 for ~230-340 ka where the data quality is excellent due to the short storage of the samples. The correlation coefficient is smaller (-0.79) for the entire record length owing to the noise in the O_2/N_2 data in the younger part. We attribute this noise to the error of the gas loss correction (see Methods); thus it is not an indication of a weaker physical link between O_2/N_2 and insolation. The physical properties of snow that cause the O_2/N_2 fractionation may also be affected by factors other than the local summer insolation, such as annual insolation, temperature or accumulation rate. We investigated this possibility by singlevariate and multivariate linear regression analyses using the summer solstice insolation, the annual mean insolation, and $\delta^{18}O_{ice}$ (a proxy for temperature that covaries with accumulation rate). The results show that the annual mean insolation and $\delta^{18}O_{ice}$ are negligible as components of the O_2/N_2 variation (Table S2). Cross spectral analyses between O_2/N_2 and the local summer insolation and between O_2/N_2 and $\delta^{18}O_{ice}$ (Fig. S5) further indicate that the O_2/N_2 variation is insensitive to orbital-scale climatic changes[S1]. We note especially that the Dome Fuji and Vostok O_2/N_2 records do not have a 100-kyr periodicity (Fig. S5 and ref. S1). Thus, no empirical support exists for the possibility of significant phase modulation of O_2/N_2 from local summer solstice insolation.

The absence of a climatic signal is possibly the result of cancellation of temperature and accumulation effects on O_2/N_2, because temperature and accumulation covary in central Antarctica. During glacial periods, low accumulation rate results in a longer duration of exposure of the snow to solar radiation, and hence more cumulative snow metamorphism. This may offset the effect of colder temperature and hence less snow metamorphism. It is thus conceivable that a small phase modulation due to climate and other non-insolation factors exists. However, excellent agreement of our

timescale with four radiometric-dated time markers (one volcanic and three abrupt CH_4 events, see below) for 92-131 kilo years before 2000 C.E. (kyr b2k) suggests that such phase modulation would be minor, if it exists.

Error estimate for the DFO-2006 timescale

The tuning tie points from the O_2/N_2 record have essentially one source of age error, which is uncertainty in the identification of O_2/N_2 peaks due to the presence of noise in the data (here peaks refer to both maxima and minima). These peaks are used as tie points in the DFO-2006 timescale and have an average spacing of ~12 kyr. Possible sources of the noise include non-orbital natural variation, measurement error and gas loss correction. A Monte Carlo simulation based on scatter of the O_2/N_2 data around the filtered curve should accurately estimate the magnitude of this uncertainty (Fig. 1). We created ~1000 pseudo data sets by adding noise to the O_2/N_2 data and detected peaks in the filtered pseudo-data to derive the variability of each peak. We used standard deviations of 1.2, 1.3, 2.0 and 0.7 ‰ for the periods 75-130, 130-210, 210-240, and 240-330 kyr b2k, respectively, for the Dome Fuji data, and 0.7 ‰ for all the Vostok data. We also conducted the Monte Carlo simulation assuming a linear relation between O_2/N_2 and the local summer solstice insolation. In this experiment, the local summer solstice insolation was scaled to match the amplitude of the O_2/N_2 record through a linear regression, resampled at intervals similar to the real data (mean interval of 1.5±0.8 kyr for Dome Fuji, 2.0±1.0 kyr for Vosotk), and then the noise was added. Relatively large uncertainty from the two methods were found at some of the peaks in the periods younger than ~230 kyr b2k where the noise levels are high or the variation of the O_2/N_2 and insolation curves are small, as expected. We report the larger of the two values for each peak for a conservative error estimate. We also examined the sensitivities of the peak positions to the outlier rejection criteria (Table S3) and found

that they are smaller than the 2σ uncertainty except for one case at 94.2 kyr b2k with
the extreme criteria (5.0 ‰).

Age estimates between tie points have two sources of error. One is associated
with the identification of tie points, as above, and the other is due to the linear
interpolation using the DFGT-2003 age model between tie points. In the first,
uncertainty between tie points is actually smaller than at the tie points themselves. For
example, the age of the midpoint between two tie points is essentially the average of
two tie point ages, each with error. For independent errors, the age uncertainty of the
midpoint would be $\sqrt{\left(\sigma_1{}^2 + \sigma_2{}^2\right)}/2$, which is smaller than the average of the errors for

the two peaks, σ_1 and σ_2. However, due to the filtering technique used for peak
identification, the errors for two adjacent tie points are partially dependent on one
another. We estimate the degree of dependence by measuring the correlation
coefficients of deviations about the mean tie point ages from the Monte Carlo
simulations. This correlation is ~0.33 between adjacent peaks (0.3 if tie points replaced
by Vostok measurements are neglected), which increases the uncertainty of the
interpolated ages by ~15% relative to those from independent tie point errors.

The second source of error between tie points ultimately comes from uncertainty
in the DFGT-2003 age model used for interpolation; however, we need only be
concerned with the accumulation of error between tie points, i.e., on timescales of
approximately 12 kyr. Error in the depth to age conversion between each timestep in
DFGT-2003 arises from both stochastic variability in the ice sheet (e.g., accumulation
rate and ice flow) and uncertainty in the model parameters. Errors due to model
parameterization would be strongly correlated from one timestep to the next. Errors due
to stochastic variability in the ice sheet could be either independent or correlated.
Therefore, we simulate age model errors in DFGT-2003 using an autocorrelated random

walk, similar to the technique used by Huybers and Wunsch (ref. S2; hereafter HW04)
for variations in sediment accumulation rates. However, our scenario differs from that
of HW04 in that we do not have multiple cores from which to estimate variability, and
our uncertainty is considerably smaller because we begin with a relatively accurate age
model rather than core depth and because the time interval between our tie points is
much smaller.

In HW04, stochastic variability (parameters of the random walk model) is
estimated by measuring the age variability of simultaneous events between different
sediment cores if sedimentation rates are assumed constant from 11 kyr to 780 kyr. The
farther an event is from the two tie points, the greater the variability is in its estimated
age. Because we have only one core, we cannot use this technique; however, we can
compare variability in the estimated ages of events between different tie points. Ideally,
we would measure and fit variability in the estimated age of events between adjacent
peaks, but the transition midpoint between peaks represents the only identifiable event
between each pair of peaks.

An insolation midpoint T_{mid} can be estimated by linear interpolation using the
midpoint t_{mid} in the DFGT-2003 age model and the ages of the two neighboring peaks
(pk1 and pk2) in the two age models.

$$T'_{mid} = T_{pk1} + (t_{mid} - t_{pk1})/(t_{pk2} - t_{pk1}) * (T_{pk2} - T_{pk1})$$

where t equals ages in DFGT-2003 and T equals DFO-2006 ages. If both age models
are errorless and O_2/N_2 response is linear, T'_{mid} estimated by interpolation exactly
equals the insolation midpoint T_{mid}. Allowing errors in DFGT-2003 but assuming that
peaks and midpoints are identified without error, the distribution of $\delta_{1,2} = (T'_{mid} - T_{mid})$
across all midpoints in the core is determined by the accumulation of errors in

DFGT-2003. Here, $\delta_{M,N}$ is the difference between the interpolated age of Mth event in the range (t_{n+N} - t_n) and the age for the same event in the insolation curve. In actuality, the distribution of δ contains contributions from DFGT-2003 age model errors and uncertainty in identification of O_2/N_2 peaks and midpoints. Because peaks and midpoints can be identified with approximately the same uncertainty (2σ error bars range from 0.8 - 3 kyr for both), we include estimates of both peak and midpoint ages in the distribution of δ. (Peaks are estimated by interpolation between adjacent midpoints.) This generates 37 events whose estimated ages can be compared with insolation ages. (We omit the events that were replaced with Vostok estimates in the final age model). To account for uncertainty in event identification, we calculate δ across all 1031 Monte Carlo simulations and observe that the standard deviation σ_1 in these 38,147 measurements of $\delta_{1,2}$ is 0.53 kyr.

The next step is to replicate the distribution of δ in a simulation of age model errors using an autocorrelated random walk. For this, we model the error ε in a 1-kyr time span of the DFGT-2003 age model as $\varepsilon_t = \alpha \, \varepsilon_{t-1} + \beta \, y_t$, where α and β are parameters and y is a normally distributed random variable with zero mean and unit variance. Uncertainty in the identification of events is simulated by imposing age offsets from the same 1031 Monte Carlo simulations used to estimate the distribution of δ in the data. However, the standard deviation of $\delta_{1,2}$ is insufficient to generate a unique solution for both α and β. To provide additional constraints for our model parameters, we also find the distribution of δ for tie points with greater spacing. As the spacing between tie points increases, so will the accumulation of age model error measured by the distribution of δ. For $\delta_{1,2}$ the tie points are at t_n and t_{n+2} and the interpolated event is t_{n+1}. We can also measure $\delta_{1,3}$ where tie points are t_n and t_{n+3} and the interpolated event is t_{n+1}. This has a nearly identical distribution to $\delta_{2,3}$ (t_{n+2} interpolated from t_n and t_{n+3}) due to symmetry; the standard deviation σ_2 of $\delta_{1,3}$ and $\delta_{2,3}$ collectively is 0.79 kyr.

Likewise we observe $\delta_{1,4}$ and $\delta_{3,4}$ to be similar to one another with a collective σ_3 of 0.87 kyr. Finally we calculate a standard distribution σ_4 of 1.15 kyr for $\delta_{2,4}$.

No pair of values for the parameters α and β exactly replicates all four of these σ values, suggesting that an autocorrelated random walk is not an entirely accurate representation of the DFGT-2003 age model error. However, we judge the model to be sufficient for the relatively small uncertainty ($2\sigma_1 \leq 1$ kyr) between closely spaced insolation peaks. Because $\delta_{1,2}$ is the only direct measure of uncertainty between adjacent insolation peaks, our parameter optimization places more weight on fitting the distribution of $\delta_{1,2}$ than higher-order δ. We select α=0.4, β=0.175 as the best-fit parameters, producing σ_1, σ_2, σ_3, and σ_4 values of 0.58, 0.75, 0.83, and 1.03 kyr, respectively. We find that the final age model uncertainty estimates have little sensitivity to moderate changes in the random walk parameter values. Fig. 1 shows the 2σ age uncertainty estimates generated by the best-fit random walk model combined with the uncertainty in peak identification. The figure accounts for tie point substitutions from the Vostok ice core and assumes that the same autocorrelated random walk model can be used to describe errors in the Vk-FGT1 age model.

Comparison with radiometric age markers

The accuracy of DFO-2006 timescale and thus the validity of the assumptions we made for constructing the timescale can ultimately be assessed by comparing it with accurate radiometric timescales of other archives using common time horizons. A volcanic ash layer in the Dome Fuji core at 1361.89 m (ref. S3, at 88.7 kyr b2k in DFGT-2003), which has been found also in the Dome C core[S4], originated from an eruption dated at 92.5 ± 2 kyr BP (before 1950 C.E.) by the $^{40}Ar/^{39}Ar$ method[S4]. This age is in agreement with the age of 92.6 ± 1.4 kyr b2k in DFO-2006. The Dongge Cave (China) speleothem record[S5] dated by the U-Th method shows abrupt activation of the

east Asian monsoon at 129.3±0.9 kyr BP, which is thought to have coincided with the abrupt atmospheric CH_4 increase at the end of Termination II. A similar $\delta^{18}O$ shift is seen also in the Peqiin Cave (Northern Israel) record at 130.9±2.7 kyr BP[S6] and in the Antro del Corchia cave (Italy) record at 129±1 kyr BP[S7]. The DFO-2006 timescale places the abrupt CH_4 increase[S8] at 130.8±1.9 kyr b2k (here 2σ uncertainty includes those of DFO-2006, CH_4 sampling resolution and ice age-gas age difference). Age agreement between the Dome Fuji CH_4 and Antro del Corchia $\delta^{18}O$ records is found also at the onset of Greenland Interstadial #23 and #24 (ref. S9), although the identification of the event #24 in the cave record seems somewhat uncertain because of rather gradual $\delta^{18}O$ change[S9]. The CH_4 increases for those events are dated at 103.1±1.4 and 109.5±1.8 kyr b2k with DFO-2006, whereas the corresponding cave $\delta^{18}O$ events are dated at 102.6±0.8 and 108.8±1.0 kyr BP, respectively. This level of agreement suggests that DFO-2006 indeed gives an accurate timescale of Antarctic climate within the estimated uncertainties. We note an ongoing study[S10] identifying Termination II onset in a West Antarctic 'horizontal ice core' close to a volcanic ash layer at 135.6±0.9 kyr BP by $^{40}Ar/^{39}Ar$ dating[S11], in agreement with the Dome Fuji result (137.0±2.2 kyr b2k).

Site temperature

The reconstructed site temperature ΔT_{site} at Dome Fuji provides supports to earlier studies. First, as observed at Vostok[S12] and Dome C[S13], the ΔT_{site} profile is close to the raw isotopic data (r^2=0.91). Second, as seen in the Vostok record[S14], the structures at glacial inceptions are modified by this correction; the glacial inceptions in the ΔT_{site} record appear to be later than those in the raw isotopic profile. This result is insensitive to the coefficients chosen for the corrections. For example, combinations of the Dome Fuji data with the coefficients for the Vostok[S12] or Dome C[S13] cores yield the same result. Third, a robust (insensitive to the coefficients) result is that the correlation

between atmospheric CO_2 concentration and temperature during all glacial inceptions is increased when accounting for both marine and deuterium-excess corrections.

Table S1. Timing of key parameters at Terminations.

Term.	Onset δ	Mid. δ	End δ	Min. I	Min. O	Min. I – Onset δ	Min. I – Mid. δ	Min. O – Onset δ
I	17.5±1.3	16.0±1.3	11.5±1.3	23.9	28.8	6	8	11
II	137.0±2.2	134.0±2.0	132.0±1.9	139.7	149.4	3	6	12
III	247.0±1.5	245.5±1.5	243.5±1.5	253.7	272.1	7	8	25
IV	344.0±1.6	339.5±1.8	337.0±1.7	346.1	351.7	2	6	8

Timings of onset, mid-transition and end of δ increase (δ^{18}O of ice; rounded to 0.5-kyr increments; error shown is 2σ dating error plus a constant identification error of 0.3 kyr) are shown, together with minima of I (insolation at 65°N on June 21) and O (obliquity) preceding the Terminations. Lag of Terminations relative to minimum I and minimum O are also shown (rounded to 1-kyr increments).

1

Table S2. Singlevariate and multivariate linear regression analyses of the Dome Fuji O_2/N_2 data using local summer insolation, local annual insolation, and $\delta^{18}O_{ice}$ (proxy for air temperature and accumulation), which can potentially affect O_2/N_2 through firn metamorphism.

(A) 234.5-338.8 kyr b2k (good data quality)

Case	Partial correlation coefficient			Coefficient of
	Inso.77°S Dec. 21	Annual insolation	$\delta^{18}O_{ice}$	determination (R^2)
1	-0.87			0.79
2	-0.87	-0.01		0.79
3	-0.85		0.05	0.80
4	-0.81	-0.05	0.07	0.80

(B) 76.5-338.8 kyr b2k (all data)

Case	Partial correlation coefficient			Coefficient of
	Inso.77°S Dec. 21	Annual insolation	$\delta^{18}O_{ice}$	determination (R^2)
1	-0.79			0.63
2	-0.78	-0.03		0.63
3	-0.78		0.05	0.63
4	-0.71	-0.11	0.13	0.64

The local summer solstice insolation was used alone (case 1) or in combination with the other variables (cases 2-4). Numbers are partial correlation coefficients for given variables, after normalizing all variables to zero mean and unit standard deviation. The coefficients of determination (R^2) are shown. The analysis was done for (A) the older part of the record where the noise in the data is small due to small gas-loss correction (Fig. S2), and (B) the entire length of the O_2/N_2 record. Note the dominance of the local summer insolation. The coefficients of determination does not increase with the addition of annual insolation and/or $\delta^{18}O_{ice}$. The result strongly suggests that the O_2/N_2 variation in orbital timescales is influenced solely by the local summer insolation, or that cancellation of opposing temperature and accumulation effects occurs.

Table S3. Sensitivity of tuning tie points to data rejection criteria.

Insolation	Rejection criteria					Max.	Min.
	2.4 ‰	3.0 ‰	**3.2 ‰**	4.0 ‰	5.0 ‰		
81.9	79.6	79.6	**79.9**	79.9	80.2	+0.3	-0.3
94.2	89.6	89.6	**90.3**	91.8	92.3	+2.0	-0.7
106.2	105.2	104.9	**104.8**	105.0	105.2	+0.4	0.0
116.8	116.3	115.7	**115.6**	115.6	115.9	+0.6	0.0
126.4	126.1	125.9	**125.9**	126.4	126.6	+0.7	0.0
137.3	138.8	138.7	**138.7**	137.9	137.9	+0.1	-0.8
150.3	153.9	153.7	**153.7**	153.7	153.7	+0.3	0.0
164.4	165.5	166.0	**166.0**	164.1	164.1	0.0	-1.9
176.3	180.3	178.0	**178.0**	177.1	177.5	+2.3	-0.9
186.4	187.1	186.8	**186.8**	186.9	187.8	+1.0	0.0
197.3	199.1	199.1	**199.1**	198.5	199.0	0.0	-0.5
209.5	211.4	210.8	**210.8**	210.8	210.6	+0.6	-0.2
240.6	241.0	241.2	**241.2**	241.3	239.6	+0.1	-1.6
252.8	253.5	253.5	**253.5**	253.4	253.6	+0.1	-0.1
268.1	268.4	268.4	**268.4**	268.4	268.3	0.0	0.0
280.9	278.5	278.5	**278.5**	278.5	278.5	0.0	0.0
290.9	288.1	288.1	**288.1**	288.1	288.1	0.0	0.0
301.6	298.4	298.4	**298.4**	298.4	298.4	0.0	0.0
313.2	310.9	310.9	**310.9**	310.9	310.9	0.0	0.0
324.7	322.5	322.5	**322.5**	322.5	322.5	0.0	0.0

The values are ages of peaks and troughs in filtered curves of summer solstice insolation at 77 °S and Dome Fuji O_2/N_2 on DFGT-2003 timescale. Maximum and minimum ages relative to the standard case (3.2 ‰ criterion) are also shown.
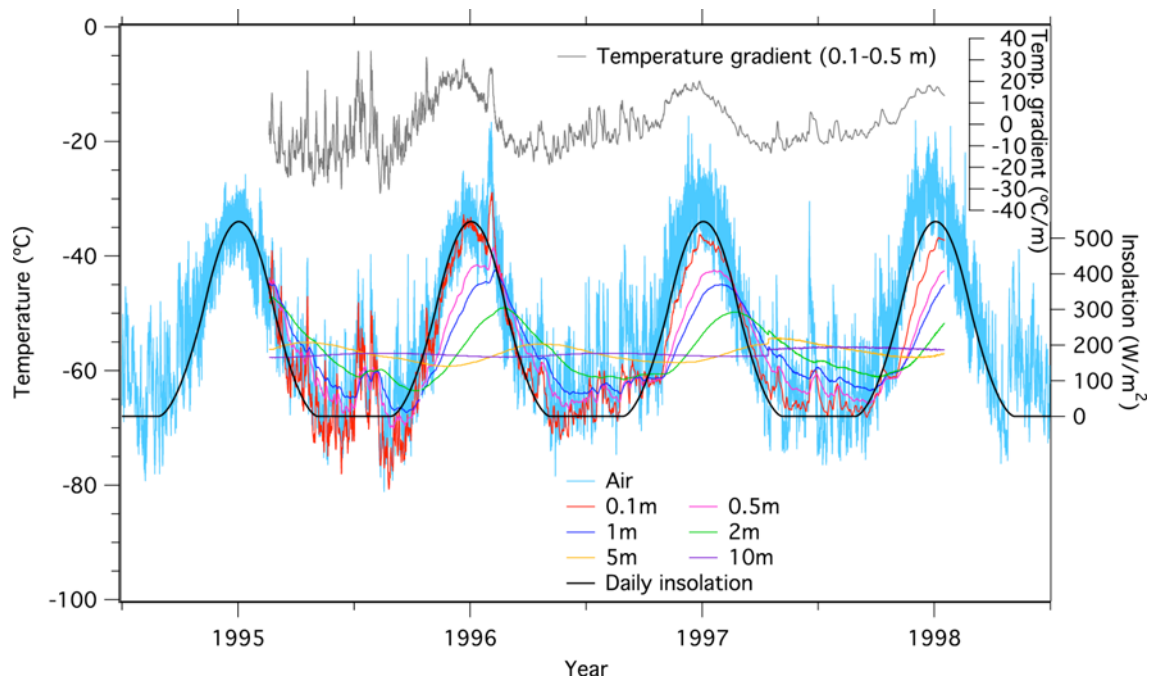
Fig. S1. Comparison between insolation (daily mean, calculated with the AnalySeries software using the Laskar 2004 solution[S15]), air temperature[S16] (observed at 3-hr intervals), snow temperature[S17-S20] (12-hr intervals) and snow temperature gradient (0.1-0.5 m) at Dome Fuji, Antarictica. Decreasing amplitudes and delayed seasonal phasings of the shallow snow temperatures in the later years are due to increasing depths of the temperature sensors by surface snow accumulation.
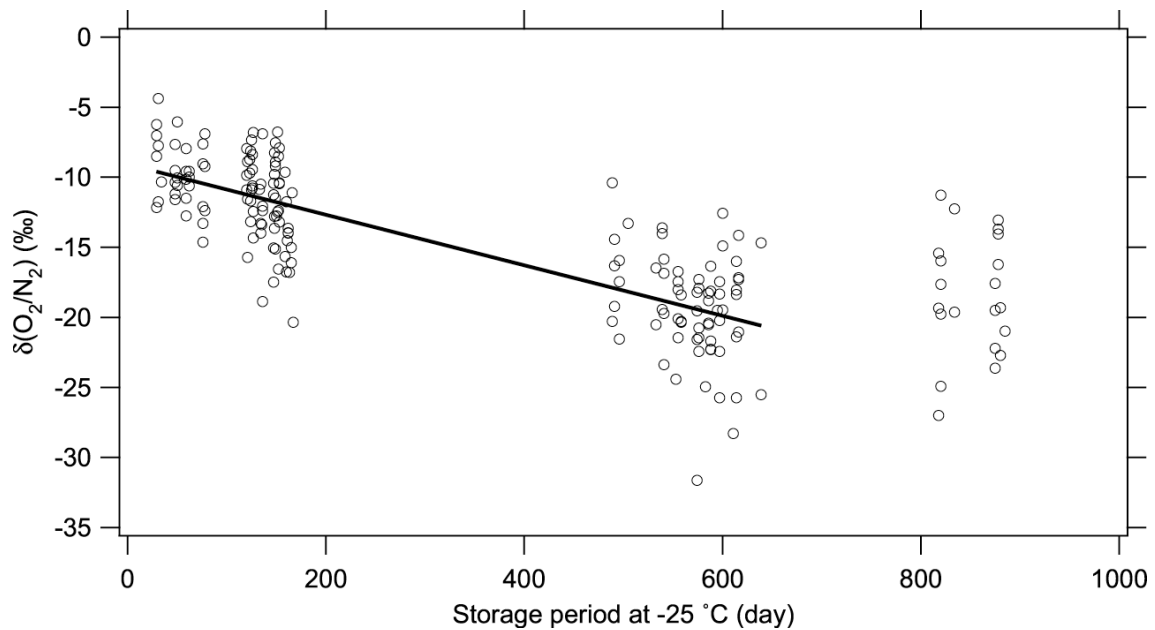
Fig. S2. O_2/N_2 of the Dome Fuji ice core plotted against the duration of storage in a freezer at –25 °C, showing a decreasing trend because of diffusive gas loss from the ice samples[S21]. The regression line is drawn through the data with storage periods of 29-639 days (slope = -0.018031 ‰ d^{-1}). The scatter on the order of ±5 ‰ around the regression line is ascribed to the natural variation of O_2/N_2 due to the fractionation during bubble formation.
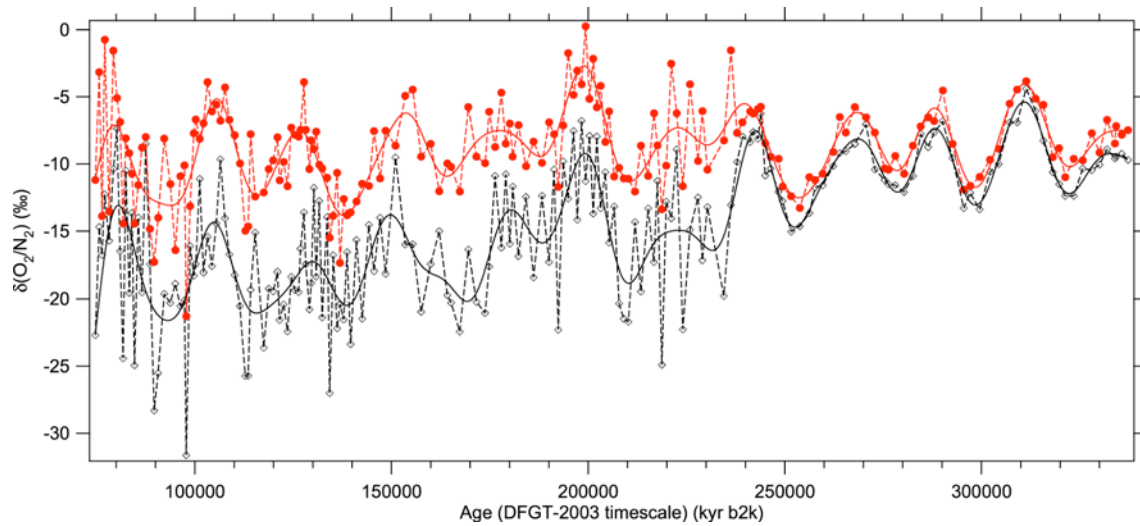
Fig. S3. Comparison of O_2/N_2 data corrected for the gas-loss fractionation during the sample storage (red circles) with uncorrected data (black diamonds). Also shown are low-pass filtered curves.
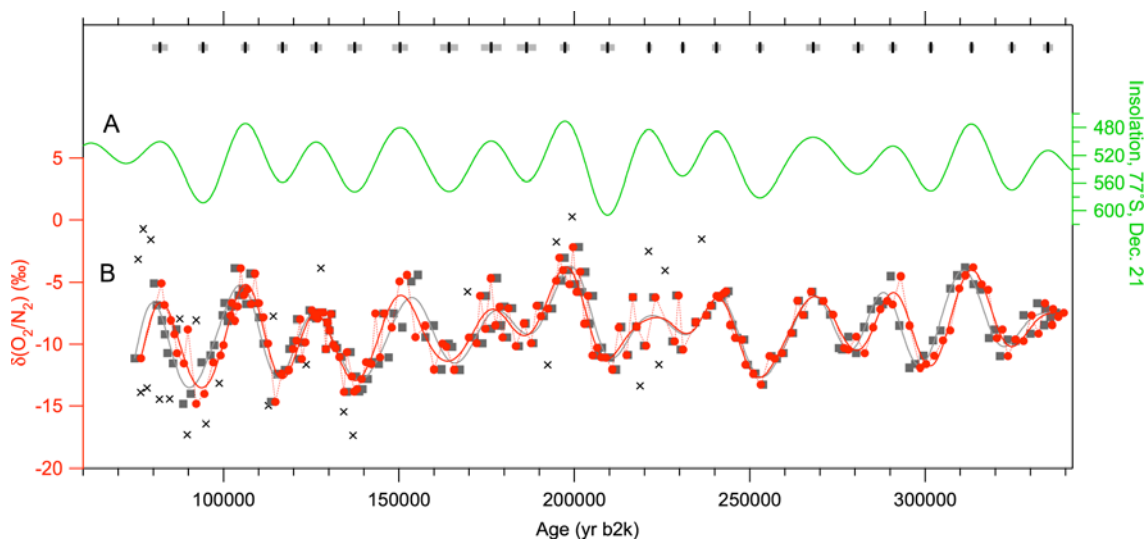
Fig. S4. Rejection of outliers in O_2/N_2 data and orbital tuning using the selected data. (A) Summer solstice insolation at 77°S used as target curve (inverted axis scale). (B) O_2/N_2 on a glaciological timescale (DFGT-2003) (gray squares) and filtered curve (gray line), rejected O_2/N_2 data (gray crosses), O_2/N_2 plotted on the O_2/N_2 timescale (DFO-2006) (red circles) and filtered curve (red line). Control points are shown at the top. Gray bars around the control points are 2σ uncertainty of the peak identification due to the noise of the data. Note that three control points at 221.2, 230.8 and 334.9 kyr b2k are adopted from the Vostok O_2/N_2 data[S1] (see text).
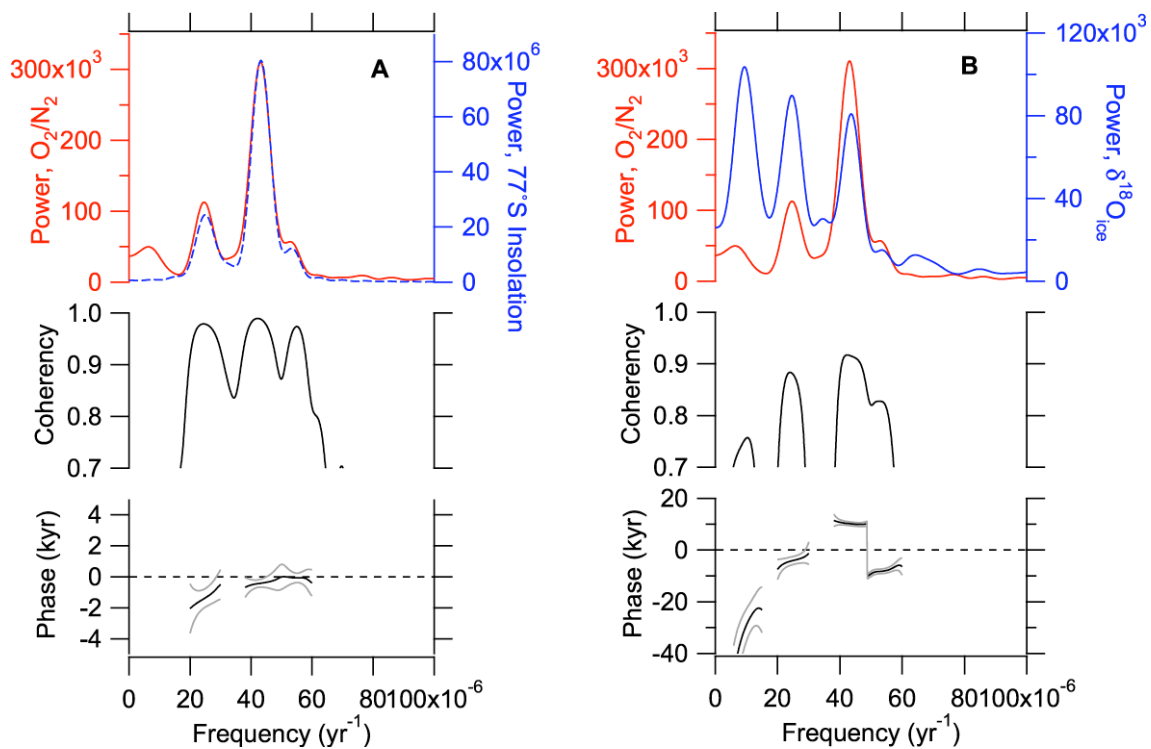
Fig. S5. Cross spectral analysis of (A) -O_2/N_2 of the Dome Fuji core (red) and summer solstice insolation at 77 °S (blue dashed line) and (B) -O_2/N_2 (red) and $\delta^{18}O_{ice}$ (blue). Positive phase means the lag of –O_2/N_2 behind the other variable. The records for 76.5-338.8 kyr b2k are interpolated at 0.1 kyr intervals, normalized to unit variance, detrended and then analyzed with the Cross Blackman-Tukey method with 50 % lag (with Analyseries software). The power spectra of O_2/N_2 and insolation (also see ref. S1) indicate that the orbital-scale O_2/N_2 variability is explained almost solely by the local summer insolation. The O_2/N_2 spectrum has a small peak at 156-kyr period without a well-defined shape. This periodicity does not relate to glacial-interglacial change of $\delta^{18}O_{ice}$ (note mismatch of peak positions, low coherency and variable phase). Also it does not appear in the power spectrum of the Vostok O_2/N_2 record for 160-385 kyr b2k[S1]. The large gas loss corrections for the young part of the Dome Fuji data might have introduced a false long-term variation.

References

S1.   Bender, M. L. Orbital tuning chronology for the Vostok climate record supported by trapped gas composition. *Earth Planet. Sci. Lett.* **204**, 275-289 (2002).

S2.   Huybers, P. & Wunsch, C. A depth-derived Pleistocene age model: Uncertainty estimates, sedimentation variability, and nonlinear climate change. *Paleoceanography* **19**, doi:10.1029/2002PA000857 (2004).

S3.   Kohno, M., Fujii, Y. & Hirata, T. Chemical composition of volcanic glasses in visible tephra layers found in a 2503 m deep ice core from Dome Fuji, Antarctica. *Ann. Glaciol.* **39**, 576-584 (2004).

S4.   Narcisi, B., Petit, J. R. & Tiepolo, M. A volcanic marker (92 ka) for dating deep east Antarctic ice cores. *Quat. Sci. Rev.* **25**, 2682-2687 (2006).

S5.   Yuan, D. X. et al. Timing, duration, and transitions of the Last Interglacial Asian Monsoon. *Science* **304**, 575-578 (2004).

S6.   Bar-Matthews, M., Ayalon, A., Gilmour, M., Matthews, A. & Hawkesworth, C. J. Sea-land oxygen isotopic relationships from planktonic foraminifera and speleothems in the Eastern Mediterranean region and their implication for paleorainfall during interglacial intervals. *Geochim. Cosmochim. Acta* **67**, 3181-3199 (2003).

S7.   Drysdale, R., Zanchetta, G., Hellstrom, J., Fallick, A. & Zhao, J. Stalagmite evidence for the onset of the Last Interglacial in southern Europe at 129 +/- 1 ka. *Geophys. Res. Lett.* **32**, doi:10.1029/2005GL024658 (2005).

S8.   Kawamura, K. Variations of atmospheric components over the past 340,000 years from Dome Fuji deep ice core, Antarctica. Ph.D. thesis, (Tohoku University, Sendai, Japan, 2001).

S9.   Drysdale, R. N. et al. Stalagmite evidence for the precise timing of North Atlantic cold events during the early last glacial. *Geology* **35**, 77-80 (2007).

S10. Popp, T. J., Sowers, T., Dunbar, N. W., McIntosh, W. C. & White, J. W. Radioisotopically Dated Climate Record Spanning the Last Interglacial in Ice from Mount Moulton, West Antarctica. *Eos Trans. AGU* **85(47)**, Fall Meet. Suppl., Abstract U31A-0015 (2004).

S11. Dunbar, N. W., McIntosh, W. C. & Esser, R. P. Physical setting and tephrochonology of the summit caldera ice record at Mt. Moulton, West Antarctica. *Geological Society of America Bulletin* **v**, in press (2007).

S12. Vimeux, F., Cuffey, K. M. & Jouzel, J. New insights into Southern Hemisphere temperature changes from Vostok ice cores using deuterium excess correction. *Earth Planet. Sci. Lett.* **203**, 829-843 (2002).

S13. Stenni, B. et al. An oceanic cold reversal during the last deglaciation. *Science* **293**, 2074-2077 (2001).

S14. Cuffey, K. M. & Vimeux, F. Covariation of carbon dioxide and temperature from the Vostok ice core after deuterium-excess correction. *Nature* **412**, 523-527 (2001).

S15. Laskar, J. et al. A long-term numerical solution for the insolation quantities of the Earth. *Astronomy & Astrophysics* **428**, 261-285 (2004).

S16. Takahashi, S., Kameda, T., Enomoto, H., Motoyama, H. & Watanabe, O. Automatic Weather Station (AWS) data collected by the 33rd to 42nd Japanese Antarctic Research Expedition during 1993 - 2001. *JARE Data Reports* **276 (Meteorology 37)**, 1-416 (2004).

S17. Kameda, T., Azuma, N., Furukawa, T., Ageta, Y. & Takahashi, S. Surface mass balance, sublimation and snow temperatures at Dome Fuji Station, Antarctica, in 1995. *Proc. NIPR Symp. Polar Meteorol. Glaciol.* **11**, 24-34 (1995).

S18. Azuma, N. et al. Glaciological Data Collected by the 36th Japanese Antarctic Research Expedition during 1995-1996. *JARE Data Reports* **223 (Glaciology 26)**, 49-66 (1997).

S19. Fujita, S., K.Kawada & Y.Fujii. Glaciological Data Collected by the 37th Japanese Antarctic Research Expedition during 1996-1997. *JARE Data Reports* **234 (Glaciology 27)**, 1-46 (1998).

S20. Motoyama, H. et al. Glaciological Data Collected by the 38th Japanese Antarctic Research Expedition during 1997-1998. *JARE Data Reports* **239 (Glaciology 28)**, 1-74 (1999).

S21. Ikeda-Fukazawa, T. et al. Effects of molecular diffusion on trapped gas composition in polar ice cores. *Earth Planet. Sci. Lett.* **229**, 183-192 (2005).